Modelling water dissociation, acid-base neutralization and ion transport in bipolar membranes for acid-base flow batteries

Arturo Ortega^a, Luis F. Arenas^{b†}, Joep J. H. Pijpers^{c‡}, Diana L. Vicencio^a, Juan C. Martínez^a, Francisca A. Rodríguez^a, Eligio P. Rivero^{a*}

Abstract

Research on flow batteries based on water dissociation and acid-base neutralization reactions at bipolar membranes is driven by the possibility of a low-cost and environmentally friendly technology. However, their application in energy storage requires a high round-trip efficiency, which has yet to be realized. In order to establish which critical factors determine their efficiency, this work examines the distribution of potential and concentration in a laboratory scale acid-base flow battery by using fundamental models. Transport mechanisms of diffusion, convection and migration were incorporated into the Nernst-Planck equation. Water dissociation during the charging step was modeled by the second Wien effect combined with the catalytic effect produced by functional groups or by catalysts present in the bipolar junction and compared to the water dissociation equilibrium model. The discharge was modeled by neutralization reaction kinetics and was also compared to the equilibrium model. All model parameters were firmly established and were determined or estimated from information available from the membrane supplier or the literature. The current-potential behavior predicted by the model for both charge and discharge closely matches experimental data and provides a lead for future work on full-scale modeling of acid-base flow batteries.

Keywords

bipolar membrane; Donnan potential; energy storage; electrodialysis; ion exchange membrane

^a Departamento de Ingeniería y Tecnología, Universidad Nacional Autónoma de México, Facultad de Estudios Superiores Cuautitlán, Av. Primero de Mayo, Cuautitlán Izcalli, Estado de México 54740, México.

^b Electrochemical Engineering Laboratory, Energy Technology Group, Faculty of Engineering and Physical Sciences, University of Southampton, Southampton, SO17 1BJ, United Kingdom.

^c Instituto Nacional de Electricidad y Energías Limpias, Reforma 113, Palmira, C.P. 62490, Edo. de Morelos, México.

[†] Present address: Institute of Chemical and Electrochemical Process Engineering, Clausthal University of Technology. Research Center for Energy Storage Technologies (EST), Am Stollen 19A, 38640 Goslar, Germany. arenas@icvt.tu-clausthal.de

[‡] Present address: First Solar, Inc. Mexico City, Mexico.

1. Introduction

Electrochemical energy storage technologies continue to gain relevance owing to the possibility of enabling the full integration of renewable power sources, such as wind and solar, into the power grid [1,2]. This is likely the most feasible path towards achieving sustainability and mitigating the environmental impact of carbon emissions. Among these technologies, those based in salinity and acidity gradients are considered promising [3,4], given the extreme abundance, low cost and low toxicity of the required substances [5,6]. In particular, reverse bipolar electrodialysis (REDBM) has been presented as an improvement over conventional reverse electrodialysis (RED) [3,7,8], which typically relies on the availability of river water and seawater [9]. REDBM is especially advantageous as it provides a significantly higher voltage per unit cell due to the large pH gradient across bipolar membranes (BM) [3,7,8]. More recently, research on REDBM has focused on flow batteries [6], i.e., rechargeable devices in which the electrolytes are continuously recirculated between membrane stacks and electrolyte holding tanks. This configuration has the advantage of scalability, modularity, safety and sizing independence between power rating and energy capacity, analogous to redox flow batteries (RFBs) [10].

As shown in Fig. 1, the acid-base flow battery (ABFB) considered in this work consists of a series of repeating flow cells formed each by a BM, an anion exchange membrane (AEM) and a cation exchange membrane (CEM). The stack of membranes is placed between two electrodes at which the interconversion of electrons and ions in solution takes place [6]. Four electrolytes are required: acid (HCl), base (NaOH), salt (NaCl) and 'rinse' (e.g. Na₂SO₄), the latter being confined to the electrode compartments. During charge, bipolar electrodialysis consumes electrical energy to produce chemical potential energy. Water is dissociated at the BM junction to form H⁺ and OH⁻ ions which are transported through its cation-exchange and anion-exchange layers to the HCl and NaOH compartments, respectively. In other words, concentrated solutions of acid and base are formed via the dilution of the salt solution. The other ions, Na⁺ and Cl⁻, are transported through AEMs and CEMs, respectively, so that the macroscopic electroneutrality is kept. During discharge, concentrated solutions of acid and base are neutralized at the BM junction through REDBM to generate electrical energy and a concentrated salt electrolyte, with ions moving in the overall opposite direction. Water

electrolysis usually takes place at the electrodes in both cases [11,12], although its substitution by electrochemical reactions of dissolved redox couples may be possible [8,13].

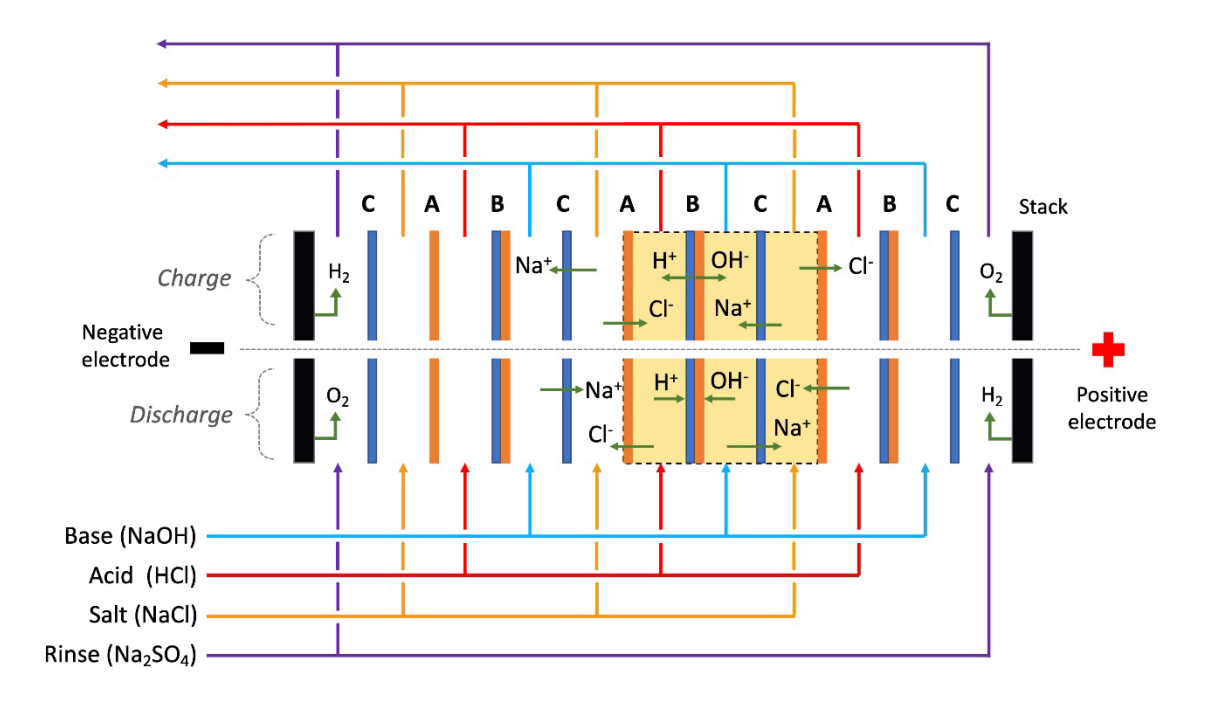


Fig. 1. Schematic of the acid-base flow battery concept and the general direction of ion transport during the charge and discharge processes. Overall products of electrode reactions are shown (water electrolysis). Three repeating unit cells are shown, one of them highlighted between dotted lines. Nomenclature: A, anion exchange membrane; B, bipolar membrane; C, cation exchange membrane.

Considering only thermodynamics, a volumetric energy density of up to 44 Wh L⁻³ could be realized by neutralizing 4 mol L⁻¹ acid and base solutions [14]. However, only a fraction of it can produce work due to non-ideal membranes, ohmic losses and diffusive fluxes, as shown for RED systems [15]. Still, an ABFB can theoretically afford an energy density of 11.1 Wh L⁻³ [12,14,16]. Early work by Van Egmond et al. reported an experimental value of 2.9 Wh L⁻³ with 1 mol L⁻¹ of acid and base [14]. Research on ABFBs has thus been directed to the improvement of the available volumetric energy density. The difference between theory and the current state of the art is mostly due to undesired transport of proton, hydroxyl and salt ions, as well as water [12,14]. In order to determine how to improve the performance of the

acid-base flow battery, experimental research has been focused on current density-voltage behavior at different acid and base concentrations with different charge and discharge conditions [12,16,17].

Moreover, the overall performance of the system is limited by the rate of water diffusion out of the BM [18]. In fact, at higher current densities, the quantity of water generated at the CEM/AEM interface can reach a higher rate than water diffusing towards the acid and base compartments, which is observed as a steep rise in the resistance of the BM. Under these conditions, the two layers of the BM suffer 'blistering' and delimitation, together with an irreversible loss of functionality. Developers of BMs have focused on increasing water permeability at concentrations greater than 2 mol L⁻¹ of acid and base at current densities over the present onset of approximately 300 A m⁻² [14,19]. Another current limitation is the loss of selectivity at acid or base concentrations over 1 mol L⁻¹ at available BMs [12].

One of the aspects that has been scarcely explored in these batteries is the modeling of the transport of ions through the membranes and solutions coupled with the reactions of water dissociation and acid base neutralization. A better understanding of these interrelated phenomena is needed in order to clarify the role played by each of the battery components. Mathematical models describing ABFB (and RED) experimental behavior are mainly based on the Nernst-Planck equation and the electroneutrality condition for solutions and membranes [19,20], although other authors have preferred using Nernst-Planck and Poisson equations [21]. The transport mechanisms of ions in liquid solutions and membranes are in principle the same. However, the convection in a membrane is negligible and very often the migration is the dominant mechanism over diffusion [22]. The presence of fixed charges on the polymer matrix of the membrane has a profound effect on the ionic flux distribution of each species in solution during operation resulting in concentration polarization close to the surface of the membrane. The degree of polarization depends on the ion transport rate and therefore on the current density. The depletion of ionic species near the surface of the membrane decreases the electrical conductivity and increases the electric field in that narrow region [23]. In the complete concentration polarization, the concentration of ions near the membrane surface approaches zero and appears new charge carriers from the water dissociation. The water dissociation process is accelerated by the catalytic effect of charged

fixed groups in anion exchange membranes. In bipolar membranes, on the other hand, the water dissociation takes place in a very thin region formed in the union of two layers of the bipolar membrane where similar conditions prevail in this bipolar junction, particularly the very low ionic concentration, high electric field, and catalytic effects [20].

Because of the complexity of modeling ion transport through a BM two different approaches have been implemented in order to represent the bipolar junction: 1) an abrupt junction and 2) a neutral layer. Indeed, the rigorous modeling of water transport through membranes still remains a challenge [24]. For example, Bassignana and Reiss employed a simplified model with symmetrical ion exchange membranes for H⁺, OH⁻ and salt ions transport through a BM, accounting for the local equilibrium condition for water dissociation at the bipolar junction [25]. Meanwhile, Kovalchuck et al. analyzed with their model the fractional charge carried by H⁺, OH⁻ and salt ions at under- and over limiting current regimens by assuming a local equilibrium for water dissociation at a bipolar junction [26].

This works presents the 2D modeling of a single ABFB unit cell that permits to simulate the flow battery charge process when a positive current is applied and its discharge process when a negative current is applied. The model can determine the concentration distribution of chemical species and electrical potential throughout a unit cell, which consists of an AEM, a BM, a CEM and its four-electrolyte compartment. As shown in Fig. 1, two of them are fed by a NaCl solution, one by a HCl solution and another by a NaOH solution. The ABFB model describes the flux of counter-ions and the electric potential as influenced by the flux of coions across the BM, plus the zero-current voltage (ZCV). This approach builds on the experience provided by the modelling of ion transport through solutions, anionic resins and AEMs for the removal of As(V) species in an ion exchange/electrodialysis flow cell developed in previous work [23]. There, water dissociation at the solution/AEM interface was successfully simulated as a neutral layer. However, the leakage coions (Na⁺ and Cl⁻) across the BM is here further implemented in order to analyze its influence on the efficiency of the ABFB. We aim to show the importance of this strategy in the future full-scale, multi-cell modeling of ABFBs.

2. Experimental

2.1 Electrolyte solutions and ion exchange membranes

Solutions of acid, base, salt and 'rinse' were prepared in volumes of 1.5 L using analytical grade reagents and deionized water with a conductivity 4.5 mS cm⁻¹. The composition and concentration of each electrolyte is presented in Table 1. The ion exchange membranes used in the study were Fumasep® FKB-PK-130 cation exchange membrane, Fumasep FAB-PK-130 anion exchange membrane and Fumasep FBM bipolar membrane (Fumatech BWT GmbH). Before their use, the membranes were immersed for 48 hours in a 0.5 mol L⁻¹ NaCl solution, which was replaced after the first 24 hours by fresh solution. Once the membranes were placed in the cell, solutions with the concentration used in the experiment (Table 1) were recirculated through the cell for 2 hours. The AEM and AEM had both a thickness of 0.13 mm, while the BM had a thickness of approximately 0.2 mm after the pretreatment.

Solution	Composition	Concentration	
Acid	HC1	0.25 mol L ⁻¹	
Base	NaOH	0.25 mol L ⁻¹	
Salt	NaCl	0.25 mol L ⁻¹	
Rinse	Na ₂ SO ₄	0.5 mol L ⁻¹	

Table 1. Solutions at the different compartments of the ABFB unit cell.

2.2 Electrodialysis stack

The electrodialysis stack used for the ABFB was an ED-100-4ES model (Fumatech BWT GmbH), consisting of two frames with ducts and two parallel plane electrodes. In this case, two dimensionally stable anodes (DSA®) were used for both the negative and positive electrodes. The projected, active surface area of the electrodes and membranes was 98 cm². As shown in Fig. 2a), the components for each repeating unit cell were placed in the following order from the negative electrode towards the positive electrode: an electrode, spacer for 'rinse' solution, CEM, spacer for salt solution, AEM, spacer for acid solution, BM and spacer for base solution. At the end, an additional CEM, a spacer for 'rinse' solution and the positive electrode. Woven mesh spacers with integrated polyvinyl chloride gaskets type ED-100-4ES (Fumatech BWT GmbH) were used. Three repeating unit cells formed the stack. In the

central unit cell, two modified acrylic polymer spacers were placed at both sides of the BM, allowing the insertion of Luggin probes, see Fig. 2b). During charge polarization (electrodialysis), the negative electrode is the cathode and the positive electrode is the anode.

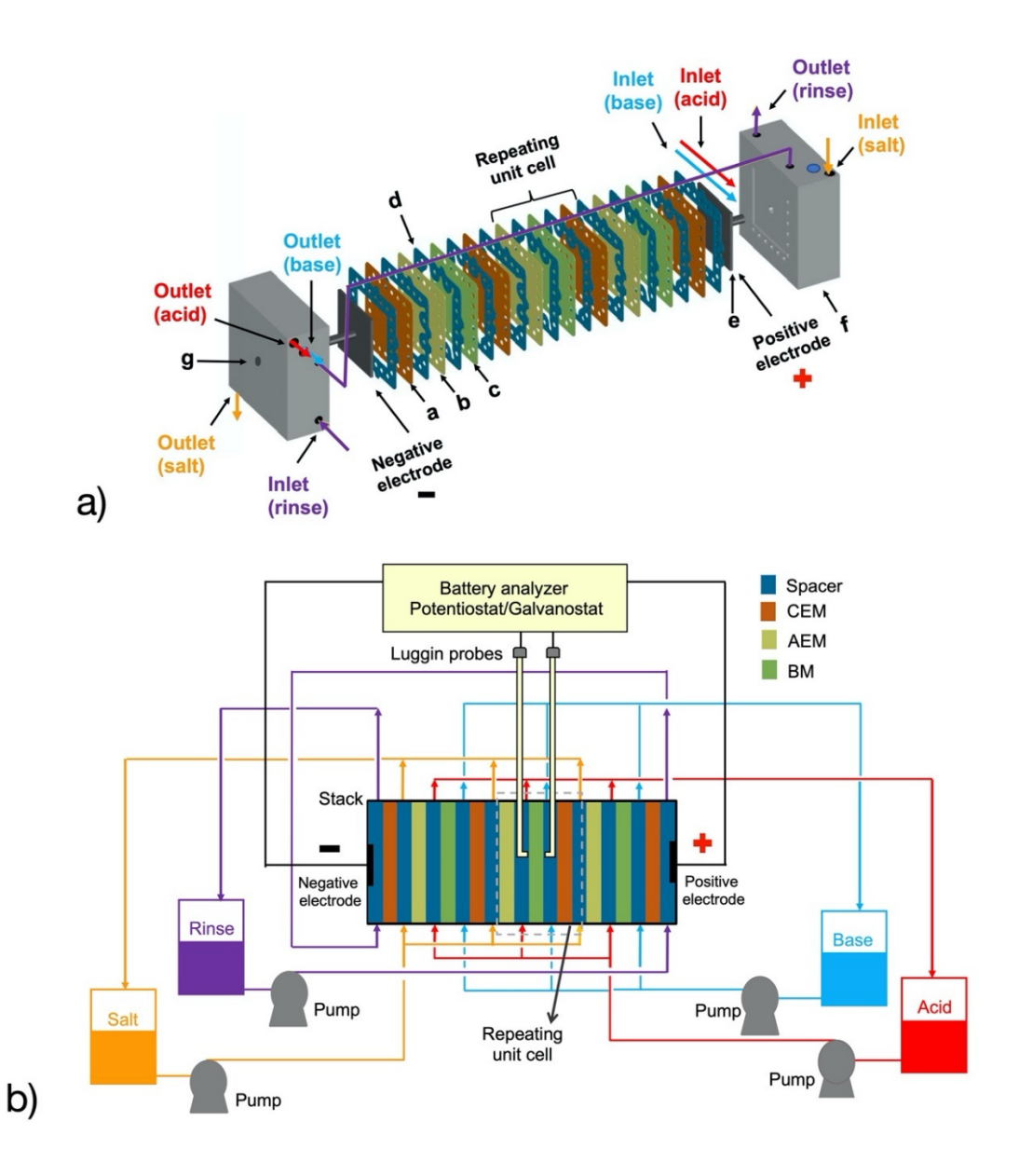


Fig. 2. Experimental arrangement for ABFB measurements. a) Exploded view of the ABFB stack. Nomenclature: a, cation-exchange membrane; b, anion-exchange membrane; c, bipolar membrane; d, spacer; e, electrodes; f, frames with ducts; g, terminals. b) Schematic of the electrolyte recirculation system for the stack coupled to a battery analyzer.

The electrolyte recirculation system is shown in Fig. 2b). It consisted of 4 PVC containers with a capacity of 5 L, one for each solution, four DMA15 flow rate sensors (Endress Hauser) as well as PVC hoses and pipes of ¼ and ½ in diameter, respectively. Each solution was recirculated by a MD-30RT centrifugal pump with 1/16 HP (Iwaki). The volumetric flow rate at the electrodialysis compartments was 20 liters per hour (LPH), corresponding to a mean linear velocity of approximately 11 cm s⁻¹. The volumetric flow rate in the electrode compartments was 150 LPH. The solutions were kept at constant temperature of 43 $^{\circ}\text{C} \pm 1$ with the help of two thermostatic baths (Thermo-Fisher Scientific) connected to the jacketed containers in series. After its assembly, the electrically disconnected experimental arrangement was set under constant recirculation of fresh electrolytes (see Table 1) for approximately 1,300 s towards reaching steady state at 43 °C. The stack was then connected to a LBT21084MC three-phase battery analyzer with a maximum capability of 10 V and 30 A (Arbin Instruments). In order to measure the difference in potential across the BM, the system was set in a four-electrode configuration and two Luggin capillaries were placed at both sides of the BM through two perforated acrylic polymer spacers. These probes communicated to saturated Ag/AgCl reference electrodes using polytetrafluoroethylene tubbing of 1.5 mm external diameter and epoxy resin seals. The working and counter electrode terminals were connected to the stack electrodes.

3. Model development

The 2D model describes the behavior of three membranes that form a single ABFB unit cell under steady state flow recirculation at all its electrolyte compartments, emphasizing the water dissociation and acid-base neutralization during both charge and discharge. Electrode reactions and the 'rinse' electrolyte are thus neglected from this study. First, hydrodynamics at the flow compartments are calculated from the Brinkman equation, then ion transport at membranes and electrolytes is given by the Nernst-Planck equation. Finally, the BM processes are considered by establishing a potential difference across a thin liquid layer between its two layers, allowing to describe ion concentration profiles, solution and membrane potential, resistive losses as well as the voltage of the repeating unit vs. current

density. Water dissociation was modeled by the second Wien effect combined with the catalytic effect at the bipolar junction and the discharge was modeled by neutralization reaction kinetics. Both were compared to the water dissociation equilibrium model. Relevant details on each component of the model are explained in the ensuing sections.

3.1 Hydrodynamic model

The flow of electrolyte inside each of the compartments of the unit cell can be described by the Brinkman equation in steady state (Eq. 1) and the continuity equation (Eq. 2). Assuming a negligible effect of concentration changes on the hydrodynamics during electrodialysis and reverse electrodialysis, the hydrodynamic model can be decoupled from the mass transfer model.

$$\frac{\rho}{\varepsilon_p} \left((\mathbf{u} \cdot \nabla) \frac{\mathbf{u}}{\varepsilon_p} \right) = \nabla \cdot \left[-p\mathbf{I} + \frac{\mu}{\varepsilon_p} (\nabla \mathbf{u} + (\nabla \mathbf{u})^T) \right] - \left(\frac{\mu}{k_{br}} + \beta_F |\mathbf{u}| \right) \mathbf{u} + \mathbf{F}$$
(1)

$$\nabla \cdot \mathbf{u} = 0 \tag{2}$$

Here, ρ is the fluid density, **u** velocity, p pressure, μ dynamic viscosity, ε_p porosity, k_{br} permeability, β_F Forchheimer coefficient (which considers density, porosity, permeability, and a dimensionless friction factor for the porosity) and **F** any external force (e.g., gravity). The boundary conditions applied to the compartments inside the repeating cell unit (delimited with broken lines in Fig. 1) of width W and high L, are:

Cell inlet, at y = 0, $\mathbf{u} \cdot \mathbf{n} = u_{in}$

Cell outlet, at
$$y = L$$
, $\left[-p\mathbf{I} + \frac{\mu}{\varepsilon_p} \mu (\nabla \mathbf{u} + (\nabla \mathbf{u})^T) \right] \mathbf{n} = -p_0 \mathbf{n}$

At the membrane surfaces, $\mathbf{u} = 0$

External boundaries, at
$$x = 0$$
 and $x = W$, $\mathbf{u} \cdot \mathbf{n} = 0$, $\left[-p\mathbf{I} + \frac{\mu}{\varepsilon_p} \mu (\nabla \mathbf{u} + (\nabla \mathbf{u})^T) \right] \mathbf{n} = 0$

3.2 Transport of ions

The mass transport flux of species *i* by diffusion, migration and convection mechanisms is given by the Nernst-Planck equation (Eq. 3).

$$\mathbf{N_i} = -(D_i \nabla C_i + z_i u_{m,i} F C_i \nabla \phi) + \mathbf{u} \cdot \nabla C_i \tag{3}$$

Where D_i is diffusion coefficient, C_i is concentration, z_i is charge, $u_{m,i}$ is ionic mobility, F is the Faraday constant, ϕ is electric potential, \mathbf{u} is velocity vector and the subscript i refers to the transported species.

The conservation of the species i in each compartment l leads to Eq. 4, where the species considered are: Na⁺ and Cl⁻ in the salt compartment (l = s), H⁺ and Cl⁻ in the acid compartment (l = a), Na⁺ and OH⁻ in the base compartment (l = b) and H⁺ and OH⁻ in the electrolyte at the BM junction (l = j).

$$\frac{\partial C_i^l}{\partial t} = -\nabla \cdot \mathbf{N}_i^l + R_i = \nabla \cdot \left(D_i^l \nabla C_i^l - \mathbf{u} C_i^l + z_i u_{m,i}^l F C_i^l \nabla \varphi^l \right) + R_i \tag{4}$$

Where t is time and R_i is the source term, which is non-zero only at the bipolar junction. Deviations from electroneutrality that can occur close to the membranes are not considered in the model. These equations must fulfill the macroscopic condition of electroneutrality at each compartment (Eq. 5).

$$\sum z_i C_i^l = 0 \tag{5}$$

Thus, the equation set formed by the conservation equations in each compartment and the electroneutrality condition defines the concentration of all ions and the electric potential. Derived quantities like the flux of each component or the current density can be calculated as well. The current density produced by the transport of ions in the liquid solution is determined with Eq. 6, where the convective term has been eliminated by applying the electroneutrality condition.

$$\mathbf{j}^{l} = F \sum z_{i} \mathbf{N}_{i}^{l} = F \sum z_{i} \left(D_{i}^{l} \nabla C_{i}^{l} + z_{i} u_{m,i}^{l} F C_{i}^{l} \nabla \varphi^{l} \right)$$
(6)

At the membranes, the charge conservation leads to Eq. 7, where current density \mathbf{j}^{m} is set through the ohmic potential drop with an isotropic conductivity σ^{m} , assuming a negligible effect of concentration gradient.

$$\nabla \cdot \mathbf{j}^m = \nabla \cdot \left\{ F^2 \sum_i \left(z_i u_{m,i}^m C_i^m \nabla \varphi^m + z_i^2 D_i^m \nabla C_i^m \right) \right\} \approx \nabla \cdot \left(-\sigma^m \nabla \varphi^m \right) = 0$$
 (7)

The coupling between the models representing electrolyte compartments to their adjacent ion-exchange membranes is carried out through the flux continuity condition and its Donnan potentials, which are the boundary conditions to the models on both sides of the solution-membrane interfaces. At the ion-exchange membrane-solution interface, the flux continuity and the Donnan potential are given by Eqs. 8 and 9.

$$\mathbf{n} \cdot \mathbf{N}_i^m = \mathbf{n} \cdot \mathbf{N}_i^l \tag{8}$$

$$\Delta \varphi_D^m = \varphi^m - \varphi^l = -\frac{RT}{z_i F} ln \frac{C_i^m}{C_i^l}$$
(9)

The remainder boundary conditions are:

Cell inlet, at y = 0, $C_i^l = C_{i,in}^l$ and $\mathbf{n} \cdot \mathbf{j}^l = 0$

Cell outlet, at y = L, $-\mathbf{n} \cdot D_i^l \nabla C_i^l = 0$ and $\mathbf{n} \cdot \mathbf{j}^l = 0$

External boundaries, at x = 0, $\varphi^s = 0$ and at x = W, $\varphi^s = V_{RU}$ and $C_i^s(W, y) = C_i^s(0, y)$

3.2 Bipolar membrane model

BMs are constituted by a cation exchange layer (BCEL) and an anion exchange layer (BAEL) and form an interface in between called membrane junction. These membranes have been employed in electrodialysis for production or recovery of acids and bases from salts due to their ability to generate H⁺ and OH⁻ ions by water dissociation in the BM junction [20], frequently with the help of a catalyst. During charging, a potential difference greater than the ZCV is applied to the electrodes so that the charged particles are forced to move from one compartment to the other to increase the concentration of HCl and NaOH. During the discharge, the ions are transported in the opposite direction and the H⁺ and OH⁻ ions reaching the bipolar junction neutralize each other forming water. See Fig. 3.

The dissociation reaction is a natural process occurring in pure water according to Eq. 10, where the forward and backward kinetic constants are k_f and k_b , respectively.

$$H_2O \rightleftharpoons H^+ + OH^- \tag{10}$$

At the equilibrium the forward reaction equals the backward reaction and the H⁺ and OH⁻ concentration reach a constant product known as dissociation constant of water (Eq. 11).

$$\frac{k_f C_{H_2O}}{k_b} = C_{H^+} C_{OH^-} = K_w \tag{11}$$

Although the water dissociation mechanism in BM junction is still controversial, e.g. see [20] and [27], it is commonly accepted that its rate depends basically on two factors: a) the magnitude of the electric field, and b) the catalytic effect of the fixed functional groups in the membrane and/or the catalyst added. The first of these factors refers to the increase of the dissociation kinetic constant by the electric field according to the second Wien effect given by Eq. 12 [27–29].

$$\frac{k_f'(E)}{k_f} = 1 + b + \frac{b^2}{3} + \frac{b^3}{18} + \frac{b^4}{180} + \frac{b^5}{2700} + \frac{b^6}{56700} + \dots$$
 (12)

$$b = 0.09636 \frac{E}{\varepsilon T^2} \tag{13}$$

Where k'f(E) is the forward rate constant for water dissociation under the effect of the electric field E, ε is the relative permittivity and T is the absolute temperature. An alternative expression analogous to the Butler-Volmer equation for describing the water dissociation rate is also available [30], although it is not used here.

The dissociation rate intensified by the electric field given by Eq. 12 is not enough to explain the very high dissociation rate found in BM [18,24]. Thus, the second factor, the catalytic effect, generates an additional increase of the dissociation rate. The kinetic scheme of water dissociation in the BM junction has been formulated to proceed through the reaction with the catalytic groups in the membrane enabling the formation of H⁺ and OH⁻ ions [31]. The analysis of the elemental kinetic steps leads to mathematical expressions of the same form that those of the free water dissociation reaction [31]. Thus, the catalytic effect can be accounted in the net dissociation reaction rate as:

$$R_{H^{+}} = R_{OH^{-}} = a(k'_{f}(E)C_{H_{2}O} - k_{b}C_{H^{+}}C_{OH^{-}})$$
(14)

In the bipolar junction, water-filled domains and pores are formed where a strong electrical field is developed upon applying a potential difference to the cell. However, the geometry of these domains is irregular, making the calculation of the electric field and ion distribution very complex. Therefore, a simplified model is necessary to describe the water dissociation in terms of the electrical field and concentration distribution of ions. The model here proposed is based on the simplified scheme depicted in Fig. 3, where a potential difference is established through a thin liquid layer between the two membrane layers. The potentials of the liquid at the interfaces with the membranes are related to the anion- and cation-exchange membranes, φ^{am} and φ^{cm} , by the Donnan potential equation (Eq. 9). Thus, the potential of the thin layer of water φ^{bj} is between the potentials at the interfaces, φ^{bj}_{am} and φ^{bj}_{cm} .

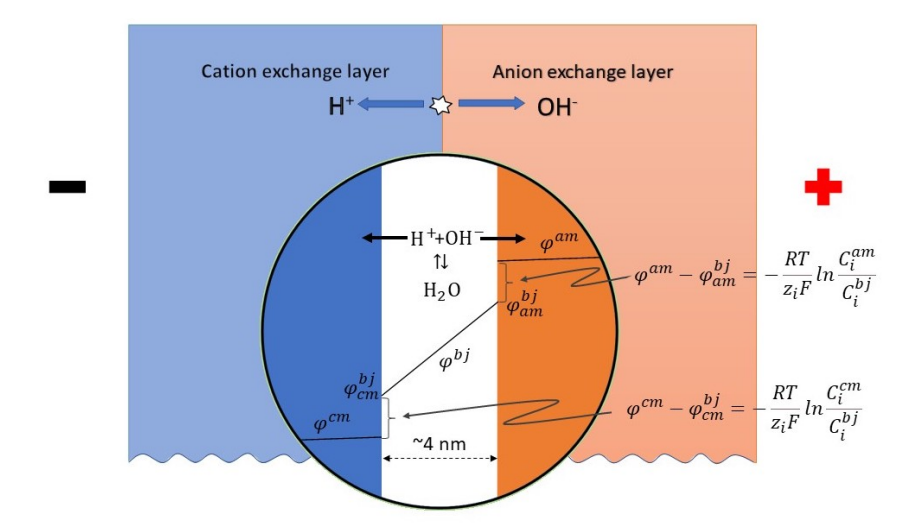


Fig. 3. Schematic of the bipolar membrane model showing its boundary conditions and ion transport during water dissociation.

3.4 Numerical solution of the model

All equations forming part of the complete model were solved numerically using COMSOL Multiphysics® 5.3. The hydrodynamic model (Eqs. 1 and 2) was solved first and its solution was stored in the program in order to be later used in the evaluation of the convective term of the mass transport model. The mass conservation equations for each species in all

compartments l (Eq. 4), along with the electroneutrality condition (Eq. 5) and the dissociation model (Eq. 11 or Eq. 14) were solved simultaneously to the charge conservation at the membranes (Eq. 7). Continuity conditions and the Donnan potential (Eqs. 8 and 9) were implemented in order to couple both types of domains (electrolyte compartments and membranes). A structured computational mesh with rectangular elements with progressively finer mesh elements towards the solution-membrane interface was used to solve the model. Four meshing variables were defined: n_y , the number of mesh elements along the y-coordinate, n_x , the number of mesh elements along the x-coordinate in each compartment, n_{mx} , the number of mesh elements along the x-coordinate in each membrane and r_x , the relation ratio between the maximum and minimum mesh element size in each compartment in the arithmetic sequence in the x-coordinate. A total of 54,000 rectangular elements (n_y =300, n_x =40, n_{mx} =10, and r_x =100) were used after inspection of the mesh size independence and verifying the well-resolved concentration profiles at the diffusion layers.

The model was solved for a given potential difference between the external boundaries of repeating unit, $V_{RU} = (\varphi^s(0, y) - \varphi^s(W, y))$. The conditions, properties and parameters required to solve the model at 25°C are given in Table 2. Temperature and concentration effects on density and viscosity of the solutions were assessed using reported correlations and available data [32–36]. The temperature dependence of the water dissociation constant K_w was determined from the data reported by Bandura et al. [37]. Also, the temperature dependence of diffusion coefficients was approximated considering that $D_i\mu/T = \text{constant}$ [38]. Correlations and details on calculations are given in Supplementary Information. The effective diffusion coefficient in the solutions, D^{l}_{i} , required in Eq. 4, can be derived through the Bruggemann correction [39], by multiplying the respective property from Table 2 by $\varepsilon_p^{1.5}$, where ε_p is the void fraction of the spacer in compartments. The ionic mobility was calculated using the Nernst-Einstein relationship ($u_{m,i} = Di/RT$). The membrane conductivities were not considered constant, since they depend on the membrane concentration of ions. Thus, these conductivities were calculated simultaneously with the iterative computing of the model through Eq. 7. The diffusion coefficients through the membranes needed to calculate their conductivities were obtained, in turn, from reported conductivity data via a procedure explained in the Supplementary Information.

Table 2. Model parameters and properties at 25 $^{\circ}\mathrm{C}.$

Parameter or condition	Value	
Cell length, L	0.1 m	
Repeating cell unit thickness, W	1.9 mm	
Membrane thickness, W_m	0.13 mm	a
Bipolar membrane layer thickness, W_{bl}	0.1 mm	a
Spacer thickness, W_s	0.48 mm	
BM junction thickness, δ	4 nm	[31]
Capacity of AEM, Cam	1.2 mol L ⁻¹	b
Capacity of CEM, Ccm	1 mol L ⁻¹	b
Capacity of bipolar membrane, C_b	1 mol L ⁻¹	С
Diffusion coefficient, D_{Na} +	$1.334 \times 10^{-9} \text{ m}^2 \text{ s}^{-1}$	[38]
Diffusion coefficient, D_{Cl} -	$2.039 \times 10^{-9} \text{ m}^2 \text{ s}^{-1}$	[38]
Diffusion coefficient, D_{H^+}	$9.312 \times 10^{-9} \text{ m}^2 \text{ s}^{-1}$	[38]
Diffusion coefficient, D_{OH} -	$5.26 \times 10^{-9} \mathrm{m}^2 \mathrm{s}^{-1}$	[38]
Density of 0.25 M NaCl, ρ_{NaCl}	1007 kg m ⁻³	[32]
Density of 0.25 M HCl, ρ_{HCl}	1003 kg m ⁻³	[33]
Density of 0.25 M NaOH, ρ_{NaOH}	1009 kg m ⁻³	[33]
Viscosity of 0.25 M NaCl, μ _{NaCl}	$9.06 \times 10^{-4} \text{ kg m}^{-1} \text{ s}^{-1}$	[34]
Viscosity of 0.25 M HCl, μ _{HCl}	$9.18 \times 10^{-4} \text{ kg m}^{-1} \text{ s}^{-1}$	d
Viscosity of 0.25 M NaOH, μ _{NaOH}	$9.20 \times 10^{-4} \text{ kg m}^{-1} \text{ s}^{-1}$	[36]
Void fraction of spacer, ε_p	0.824	e
Ionic product for water, K_w	1.02×10^{-14}	[37]
Forward water dissociation constant, k_f	$2.7 \times 10^{-5} \text{ s}^{-1}$	[30]
Backward water dissociation constant, k_b	$1.5 \times 10^{11} \text{ L mol}^{-1} \text{ s}^{-1}$	[30]

a) From supplier data.

b) From supplier data assuming a density of 1000 kg $\mbox{m}^{\mbox{-}3}.$

c) Assumed from the values of AEM and CEM.

- d) From correlation of reported data.
- e) Calculated from the geometry of woven mesh spacers.

4. Results and discussion

4.1 Modelling and experimental voltage in bipolar membrane

Fig. 4 shows the comparison of modelling results and experimental data for the voltage between the Luggin probes, placed in the compartments at both sides of the bipolar membrane, see Fig. 2b), against current density calculated as the external current divided by the active area. During charge, the experimental voltage shows a good agreement with the equilibrium dissociation model (EWD), see continuous lines. However, it is evident that the experimental voltage during discharge decays faster than the model at current densities over 350 A m⁻², most likely due to the increasing water accumulation at the BM junction. It should be noted that the modelled voltage represents the potential difference at the same points where the Luggin capillaries were physically placed, and the current density was obtained by averaging the current density over the whole membrane surface, which may lead to a small deviation.

The variation of voltage with current density depicted in Fig. 4 is a measure of the resistances for ion transport through the bipolar membrane and the diffusion layers on both sides of the BM as well as those of the water dissociation and acid-base neutralization reactions. These resistances impact in the energy efficiency of the ABFB. The experimental voltage efficiency defined as the ratio of the discharge to charge voltage of the data in Fig. 4 produces an almost linear relationship with respect to the current density. Thus, the voltage efficiency is 70% at 200 A m⁻² and decreases by ca. 30% every 200 A m⁻². The EWD model predictions agree closely with experimental voltage efficiency at low current densities and deviate slightly at higher current densities over 350 A m⁻² as in the case of discharge voltage.

The dotted lines correspond to two cases of the second Wien effect with catalyzed water dissociation (SWE-CWD) model. Each case corresponds to a value where *a* in Eq. 14 is constant. Clearly the SWE-CWD model approaches to the EWD model as the catalytic effect increases and both models coincide for a sufficiently high value of the *a* parameter.

According to the results shown and for all practical purposes, the catalytic effect on the BMs is strong enough to assume an equilibrium of water dissociation reaction. Thus, the subsequent simulations are performed through the EWD model only.

On the other hand, the ZCV calculated with the EWD model was 0.764 V, while the experimental value was 0.743 V, a difference of 0.021 V. This difference in the ZCV causes the model prediction to fall slightly above the experimental data in Fig. 4. Such a difference between the calculated and measured ZCV was also reported by Xia et al. [12], who observed an experimental value of approx. 0.726 V at 43°C and attributed it to the crossflow of coions. Thus, the Na⁺ coions pass through the anionic layer of the bipolar membrane from the NaOH compartment to the bipolar junction and from there to the HCl compartment through the cationic layer of the BM. Similarly, the Cl⁻ ions cross the BM in opposite direction. These mechanisms decrease the Donnan potential by reducing the concentration of H⁺ ions in the cationic layer and OH⁻ in the anionic layer of the BM at the interfaces with the bipolar junction.

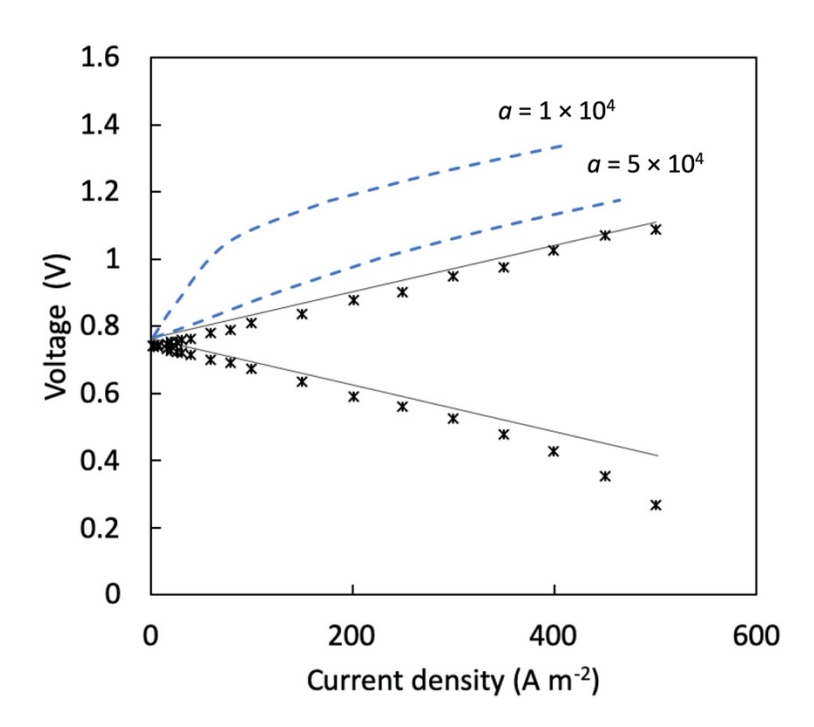


Fig. 4. Comparison of model results and experimental current density and potential difference data between two Luggin capillaries located on both sides of the bipolar membrane; 2nd Wien effect with different catalytic effect (dotted lines) and equilibrium dissociation model (continuous lines).

4.2 Modelling the behavior of ABFB

The concentration profiles in the diffusion layers at both sides of the BM at a cross-section of the cell at a height of L/2 are shown in Fig. 5 at various current densities during the charge (positive current densities) and discharge (negative current densities). This follows the expected behavior: During charging, the H⁺ and OH⁻ ions generated at the BM junction are transported to the HCl and NaOH compartments, through the cationic and anionic layers of the bipolar membrane, respectively, causing an increase of ion concentrations in the diffusion layers. During discharge the process is reversed and the H⁺ and OH⁻ ions, coming from the HCl and NaOH compartments respectively are transported to the bipolar junction where they are neutralized. It is clear that a higher concentration polarization is achieved in the NaOH compartment than in HCl compartment, for a given current density, due to the higher mobility of H⁺ ions in comparison to OH⁻ ions.

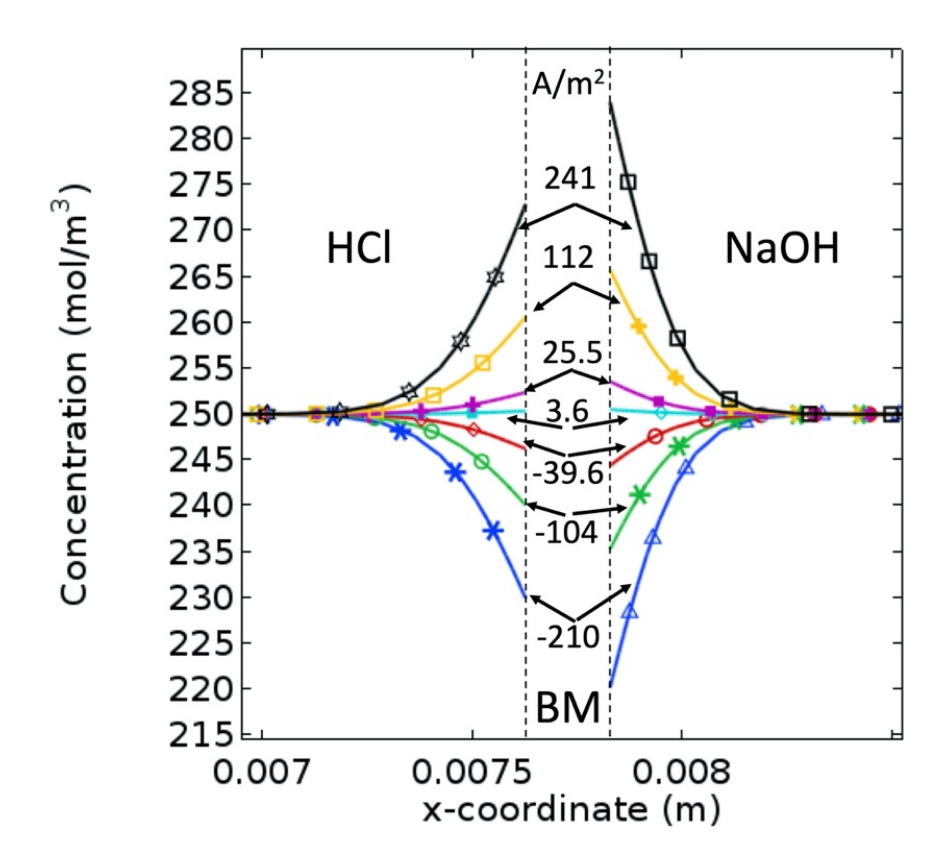


Fig. 5. Ion concentration profiles in the diffusion layers at both sides of the bipolar membrane in the cross-section at a height of L/2 calculated with ion transport and equilibrium water dissociation model. The profiles at both sides of the bipolar membrane correspond to the current density values indicated in the center of the plot.

The high concentration of H^+ and OH^- ions at the electrolyte in the interfaces with the BM during the charging stage produces a diffusion flux from the interface to the bulk solutions in both HCl and NaOH compartments. This diffusion flux diminishes away from the membrane until vanishing in the bulk solution. See Fig. 6. The high ionic concentration causes greater conductivity at the electrolyte close to the membrane and a smaller electric field in the *x*-direction, as shown by the partial derivative of the potential in Fig. 6. These variations of concentration and electric field affect the migration transport, although their effects partially counteract each other and a net decrease of migration flux close to the

membrane is observed under the prevailing conditions. Thus, ions are transported by a migration mechanism in the bulk and only in the region near the membrane the diffusion mechanism becomes important. At the interface with the membrane both fluxes are equal for a complete exclusion of coions. The total flux in the *x*-direction, i.e. the sum of fluxes by migration and diffusion, is greatest near the membrane highlighting the importance of this region for understanding the performance of ABFBs. During discharge, the concentration of ions decreases near the membrane surface, decreasing the conductivity and increasing the electric field. As in the previous case, the diffusion flux increases near the membrane and migration decreases, the net result being again a greater flux near the membrane than in bulk solution.

Fig. 7 shows the electric potential in a cross-section at a half of the height of repeating unit cell. The three compartments for HCl, NaOH and NaCl solutions, an AEM, a CEM and a BM with its two layers (BCEL and BAEL) are visible. The potential is displayed in each medium indicated in Fig. 7 for the charge process in the upper lines and for the discharge process in the lower lines at a current density of 200 A m⁻², a flow rate of 20 LPH and a concentration of 0.25 M for all solutions. The ZCP of the repeating unit cell calculated by interpolation of the current vs. voltage model predictions is 0.764 V. This value is equal to the ZCP calculated at the position of Luggin probes (see Fig. 4).

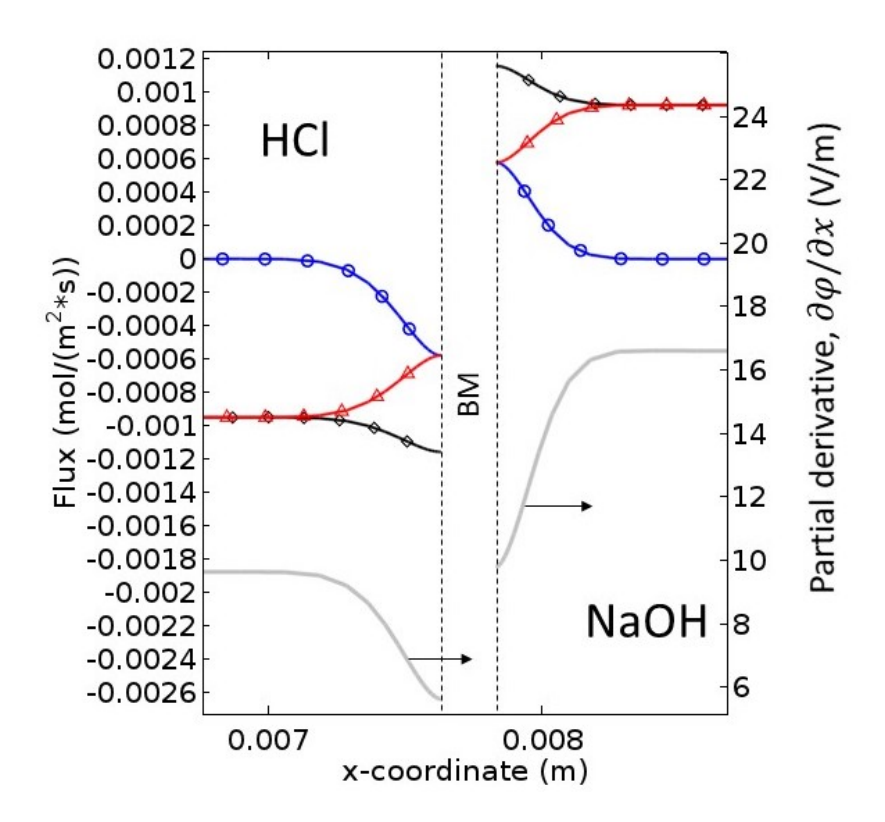


Fig. 6. Fluxes of H⁺ and OH⁻ in the *x*-direction in the adjacent layers of bipolar membrane (BM) during charge at 112 A m⁻² at a half of the cell height; (\circ) diffusion, (Δ) migration, and (\diamond) total flux.

According to the model, the potential above ZCP (V_{RUC} - ZCP) required to move the ions through both membranes and solutions for a charge step at a current density of 200 A m⁻² is 0.29 V, i.e. the potential difference in the repeating unit cell V_{RUC} is 1.05 V. During discharge a potential difference from the ZCP is also required to move the ions through the components of the cell in the opposite direction. This difference is slightly larger than that for charging owing to small changes in conductivity of solutions and membranes. As noted in Fig. 7, an overpotential from ZCV is required due to the ohmic losses at the membranes and electrolyte solutions, and to compensate for small differences in Donnan potentials arising from concentration polarization. The model also shows the distribution of average potential drops among the components of the repeating unit cell: 19% for the three electrolyte compartments,

60% for membranes, and 16% for bipolar junction. The overpotential is a critical parameter in energy storage applications due to its impact on efficiency. For the results in Fig. 7, the voltage efficiency of a unit cell, defined as the ratio of the potential V_{RUC} in discharging to that in charging, is 46% at 200 A m⁻². It is evident that the limiting components in the unit cell are the membranes.

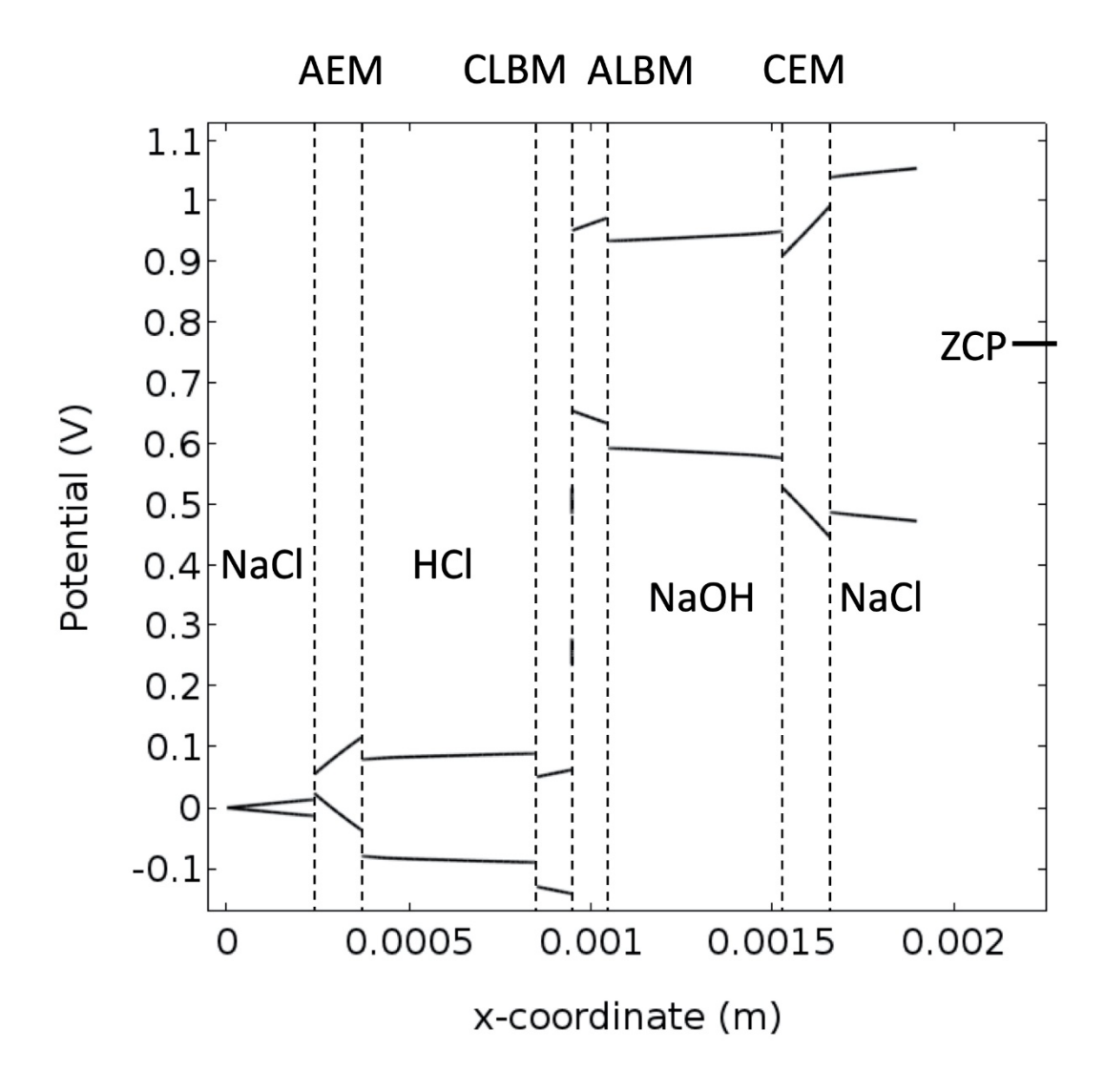


Fig. 7. Electric potential distribution in the cross section of the cell at a height of L/2 for 200 A m⁻², HCl, NaOH and NaCl 0.25 M, 20 LPH.

The bidimensional distribution of resistive losses per volume or power density losses (kW m⁻³) is illustrated for the charging process of the cell at 1.57 V shown in Fig. 8. Again, the greatest losses are found in the membranes and among them the CEM has the greatest losses followed by the AEM, then by the ALBM and finally the CLBM. The difference is caused by the concentration and mobility of predominant ions in each membrane, which have an influence on their conductivity. Thus, membranes with a larger concentration of ions with higher diffusion coefficient and mobility (in the order H⁺ > OH⁻ > Cl⁻ > Na⁺) exhibit lower losses. Likewise, the difference in power density losses among the compartments is due to the same order of mobility of ions. There are also differences between the upper and lower part of the repeating unit cell caused by concentration changes that produce a slight increase of membrane conductivity and current density in the lower part. These concentration changes in membranes occur due to the concentration polarization in the electrolyte which is more developed in the upper region of the cell. The strongest effect of concentration polarization is observed in the NaCl compartment in the neighborhood of the CEM. These changes are associated with the formation of stronger electric fields and cause greater energy dissipation. On the contrary, on the other side of the CEM, only a slightly increase in resistive losses is observed in the NaOH compartment. During the discharge process the opposite takes place, i.e. a higher dissipation occurs in the NaOH compartment close to the AEM. The slight decrease in resistive losses in the electrolyte layer adjacent to the BM in the HCl compartment is also noticeable in Fig. 8.

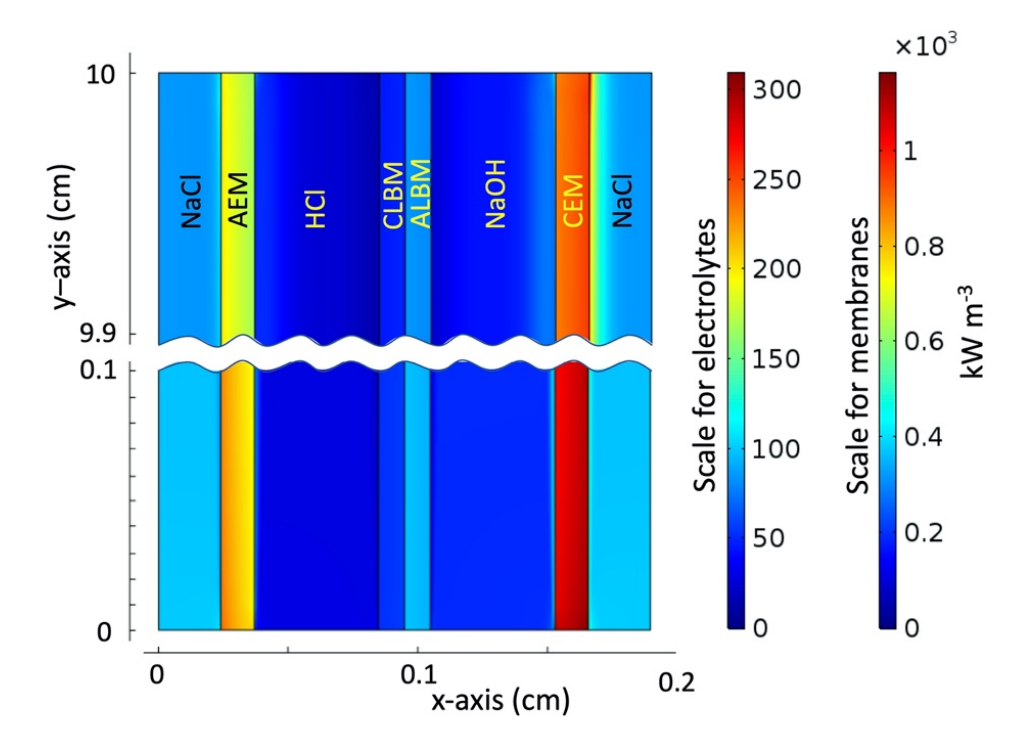


Fig. 8. Resistive losses at the top and bottom of the repeating unit; charge at $V_{RUC} = 1.57 \text{ V}$ and 0.25 mol L^{-1} .

4.3 Concentration, temperature and flow rate effects

Fig. 9 shows the concentration, temperature and flow rate effects on the voltage efficiency and power density generated in a repeating unit cell according to the model. Voltage efficiency was calculated with charge and discharge voltages for the same current density. The expected efficiency loss with increasing current density is more intense at lower temperature and lower electrolyte concentration, as shown by Fig. 9 a) and Fig. 9 b), respectively. The power density increases together with current until reaching a maximum and then decreases. A temperature increase causes the maximum power density to be reached at a higher current density. This is explained by the diminution in electrolyte viscosity and the improvement of mass transport owing to the increase of diffusion coefficient and ionic mobility according to Nernst-Einstein equation. Equally, the electrolyte conductivity increases, lessening the ohmic potential drop. A minor consequence of temperature increase

is the diminution of concentration polarization, which causes slight change in the Donnan potential.

Regarding the ion exchange membranes, including the BM, temperature increase improves membrane conductivity. Thus, temperature increases the power density due to the higher discharge potential reached. This is a consequence of the lower ohmic potential drop and changes in Donnan potential, dissociation constant K_w and ZCV. Actually, K_w increases from 1.02×10^{-14} at 25 °C to 3.63×10^{-14} at 43 °C and ZCV increases from 0.753 V at 25 °C to 0.764 at 43 °C. Changes in electrolyte concentration, even only at the interface membrane-electrolyte, modify the concentration of mobile ions in the membranes, according to the Donnan equation. This concentration of mobile ions in the membranes also affect their conductivity.

The flow rate has only a minor effect on efficiency and power density, as shown by Fig. 9 c). Among the three mechanisms of mass transport, diffusion, migration and convection, migration is dominant. Thus, concentration gradients are developed close to the membranes giving rise to diffusion fluxes that increase rapidly within a very short distance as shown in Fig. 5. The fixed electric charges in the ion-exchange membranes generate a higher mass transport number, compared with that of the adjacent solution, and produce such concentration gradients. The concentration of ions diminishes in the solution adjacent to membranes where ions enter the membrane and increases where ions leave the membrane. Thus, an increasing diffusion flux of both counterions and coions towards the membranes is developed close to their surface.

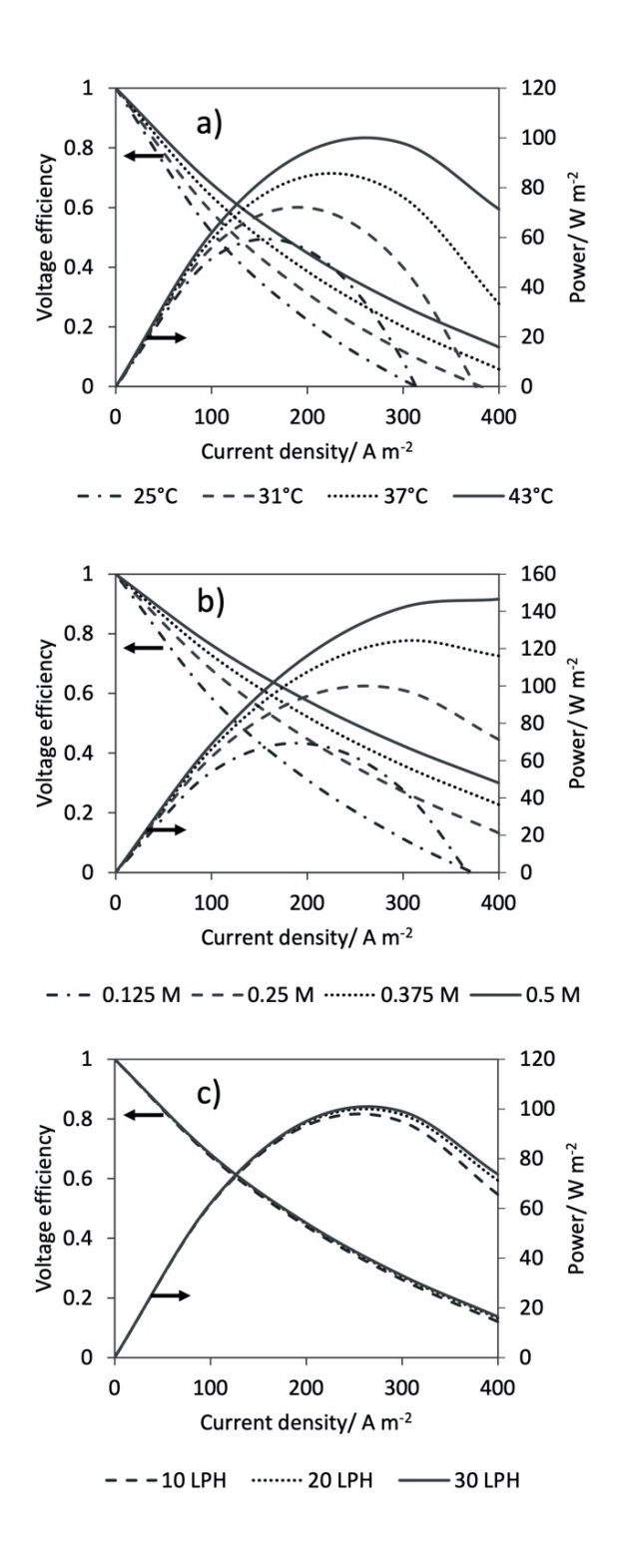


Fig. 9. Efficiency and power of repeating unit cell as a function of current density at: a) different temperatures at 0.25 M and 20 LPH b) different electrolyte concentrations at 43 °C and 20 LPH, and c) different flow rates at 43 °C and 0.25 M.

For the BM and under the model here considered, the migration fluxes reach the same value of the diffusion fluxes at the interface with the membrane, see Fig. 6, in the same direction for counter ions and in opposite direction for co ions. In this way, the total flux is twice the diffusion flux at the interface of the BCEL and BAEL for H⁺ and OH, respectively. Also, the concentration polarization is affected by the flow rate to a minor degree [40]. Thus, no significant difference on voltage efficiency and power density at the three flows depicted in Fig. 9 c) is observed, indicating that the storage energy process is practically independent of the electrolyte velocity, specially a low current density. This behavior agrees with the results reported by Sharafan et al. [41]. Indeed, at low current density, far from the limiting current density, the ionic fluxes and cell potential V_{RUC} are almost independent of flow rate, but a high current density the fluxes show a slightly flow rate effect leading to a higher voltage efficiency and power density with higher mass transport.

The model predicts a strong variation in voltage efficiency in the repeating unit cell depending on temperature, electrolyte concentration, and current density. For the conditions shown in Fig. 9, the voltage efficiency varies between 22% and 76% in a current density range of 100 to 200 Am⁻². These values were obtained for the properties of the membranes used in the experiments. However, they can be increased by decreasing the resistance of the membranes (increasing the conductivity and decreasing the thickness) and improving their properties, particularly the proton selectivity of the BM [42]. This can be achieved by increasing the permselectivity, water permeability, water dissociation rate and ion exchange capacity without losses in mechanical and chemical stability, which can produce gradual loss of ion exchange capacity or permselectivity.

The energy efficiency of a full ABFB with multiple repeating units and electrode reactions is lower that its voltage efficiency due to the energy losses caused by the electrode overpotentials, the shunt currents through the internal stack manifolds and the pump energy consumption, among the most detrimental factors [24]. However, given that the model is concerned with the behavior of a representative unit cell under the reaction environment expected in upscaled device, the energy consumption of the pumps is neglected in this case

as it is more appropriate for the assessment of energy efficiency at the energy storage system level.

Conclusions

An ion transport model coupled to water dissociation and acid-base neutralization reactions in a liquid film at the BM junction has been developed. A comparison of the model against experimental data can establish that the combined effect of catalysis and strong electric field causes an efficient water dissociation equivalent to an equilibrium reaction. Thus, the EWD model combined with the ion transport given by Nernst-Planck equation, allowed to predict the potential vs. current potential behavior of the bipolar membrane and adjacent electrolyte films. The modeling results describe the distribution of important characteristics as well as the contribution of different transport mechanisms. These distributions allow to identify ineffective regions in the ABFB. In essence, significant improvements are required to the membranes in order to produce a viable technology. Thus, the model shows to be a very useful tool for analysis of ABFB performance. The analysis of transport mechanisms of convection, migration and diffusion point out the important changes that take place in the electrolyte films adjacent to membranes on electric field, concentration gradient and ion fluxes. However, such changes have minimal effect on voltage at low current densities. The model can be also useful to search for better operational conditions and to make estimations of performance parameters as efficiency, power density and energy dissipation.

Further work

Considering that the average potential loss in a repeating unit is ca. 60% for the three membranes and 16% for the BM bipolar junction, efforts should focus on the development of tailored membranes if ABFBs are to become a feasible technology. For instance, the thickness of the BCEL and BAEL could be reduced and their chemical composition and structure optimized (e.g. polymer type, equivalent weight, ion exchange capacity, permselectivity, addition of a bilayer [43]). This would reduce their resistivity and possibly increase the rate of water diffusion out of the BM during discharge. The strategy is valid also

for AEM and CEM in the repeating units. Regarding the composition of the membranes, this should contemplate improved or sufficient chemical stability and mechanical resistance, even if their thickness is decreased. The concentration and type of catalyst at the BM junction could also be modified so as to achieve lower water-splitting overpotentials [20]. Although the design trade-offs between these characteristics are challenging, improvements are certainly possible, since the membranes presently available in the market have been designed for conventional electrodialysis operations (e.g. large-scale desalination or manufacture of specialized salts [42]) and not for energy storage.

Acknowledgements

This research was funded by CONACYT-SENER Fondo de Sustentabilidad Energética under project 292862. F. A. Rodríguez would like to thank the complementary support by PIAPI grant 2044.

Abbreviations

ABFB, Acid base flow battery

AEM, Anion exchange membrane

BAEL, Bipolar anion exchange layer

BCEL, Bipolar cation exchange layer

BM, Bipolar membrane

CEM, Cation exchange membrane

EWD, Equilibrium dissociation model

RED, Reverse electrodialysis

REDBM, Reverse electrodialysis with bipolar membrane

RFB, Redox flow battery

References

- [1] J. Moseley, P. T.; Garche, ed., Electrochemical Energy Storage for Renewable Sources and Grid Balance, Elsevier, 2015. doi:10.1016/C2012-0-01253-7.
- [2] M. Arbabzadeh, J.X. Johnson, G.A. Keoleian, P.G. Rasmussen, L.T. Thompson, Twelve Principles for Green Energy Storage in Grid Applications, Environ. Sci. Technol. 50 (2016) 1046–1055. doi:10.1021/acs.est.5b03867.
- [3] J. Pretz, E. Staude, Reverse electrodialysis (RED) with bipolar membranes, an energy storage system, Berichte Der Bunsengesellschaft Für Phys. Chemie. 102 (2010) 676–685. doi:10.1002/bbpc.19981020412.
- [4] H. Tian, Y. Wang, Y. Pei, J.C. Crittenden, Unique applications and improvements of reverse electrodialysis: A review and outlook, Appl. Energy. 262 (2020) 114482. doi:10.1016/j.apenergy.2019.114482.
- [5] M.A. Morales-Mora, J.J.H. Pijpers, A.C. Antonio, J. de la C. Soto, A.M.A. Calderón, Life cycle assessment of a novel bipolar electrodialysis-based flow battery concept and its potential use to mitigate the intermittency of renewable energy generation, J. Energy Storage. 35 (2021). doi:10.1016/j.est.2021.102339.
- [6] R. Pärnamäe, L. Gurreri, J. Post, W.J. van Egmond, A. Culcasi, M. Saakes, et al., The acid–base flow battery: Sustainable energy storage via reversible water dissociation with bipolar membranes, Membranes (Basel). 10 (2020) 1–20. doi:10.3390/membranes10120409.
- [7] E.K. Zholkovskij, M.C. Müller, E. Staude, The storage battery with bipolar membranes, J. Memb. Sci. 141 (1998) 231–243. doi:10.1016/S0376-7388(97)00306-2.
- [8] Y. Mei, L. Liu, Y.C. Lu, C.Y. Tang, Reverse Electrodialysis Chemical Cell for Energy

- Harvesting from Controlled Acid-Base Neutralization, Environ. Sci. Technol. 53 (2019) 4640–4647. doi:10.1021/acs.est.8b06361.
- [9] M. Tedesco, A. Cipollina, A. Tamburini, G. Micale, Towards 1 kW power production in a reverse electrodialysis pilot plant with saline waters and concentrated brines, J. Memb. Sci. 522 (2017) 226–236. doi:10.1016/j.memsci.2016.09.015.
- [10] L.F.. Arenas, J.J.H. Pijpers, Hydraulic aspects of redox flow batteries: flow fields and hydraulic circuits, in: L.F. Cabeza (Ed.), Encyclopedia of Energy Storage, Elsevier Inc., 2021. doi:10.1016/B978-0-12-819723-3.00073-1.
- [11] H. Strathmann, Electrodialysis, a mature technology with a multitude of new applications, Desalination. 264 (2010) 268–288. doi:10.1016/j.desal.2010.04.069.
- [12] J. Xia, G. Eigenberger, H. Strathmann, U. Nieken, Flow battery based on reverse electrodialysis with bipolar membranes: Single cell experiments, J. Memb. Sci. 565 (2018) 157–168. doi:10.1016/j.memsci.2018.07.073.
- [13] J.H. Kim, J.H. Lee, S. Maurya, S.H. Shin, J.Y. Lee, I.S. Chang, et al., Proof-of-concept experiments of an acid-base junction flow battery by reverse bipolar electrodialysis for an energy conversion system, Electrochem. Commun. 72 (2016) 157–161. doi:10.1016/j.elecom.2016.09.025.
- [14] W.J. Van Egmond, M. Saakes, S. Porada, T. Meuwissen, C.J.N. Buisman, H.V.M. Hamelers, The concentration gradient flow battery as electricity storage system: Technology potential and energy dissipation, J. Power Sources. 325 (2016) 129–139. doi:10.1016/j.jpowsour.2016.05.130.
- [15] F. Giacalone, P. Catrini, A. Tamburini, A. Cipollina, A. Piacentino, G. Micale, Exergy analysis of reverse electrodialysis, Energy Convers. Manag. 164 (2018) 588–602. doi:10.1016/j.enconman.2018.03.014.
- [16] J. Xia, G. Eigenberger, H. Strathmann, U. Nieken, Acid-base flow battery, based on reverse electrodialysis with bi-polar membranes: Stack experiments, Processes. 8 (2020). doi:10.3390/pr8010099.
- [17] W.J. van Egmond, M. Saakes, I. Noor, S. Porada, C.J.N. Buisman, H.V.M. Hamelers,

- Performance of an environmentally benign acid base flow battery at high energy density, Int. J. Energy Res. 42 (2018) 1524–1535. doi:10.1002/er.3941.
- [18] H. Strathmann, J.J. Krol, H.J. Rapp, G. Eigenberger, Limiting current density and water dissociation in bipolar membranes, J. Memb. Sci. 125 (1997) 123–142. doi:10.1016/S0376-7388(96)00185-8.
- [19] A. Culcasi, L. Gurreri, A. Zaffora, A. Cosenza, A. Tamburini, G. Micale, On the modelling of an Acid/Base Flow Battery: An innovative electrical energy storage device based on pH and salinity gradients, Appl. Energy. 277 (2020) 115576. doi:10.1016/j.apenergy.2020.115576.
- [20] Y. Tanaka, Bipolar Membranes Electrodialysis, in: Y. Tanaka (Ed.), Ion Exchange Membranes. Fundamentals and Applications, 1st ed., Elsevier, Amsterdam, 2007: pp. 405–436. doi:10.1016/S0927-5193(07)12017-9.
- [21] R. Femmer, A. Mani, M. Wessling, Ion transport through electrolyte/polyelectrolyte multi-layers, Sci. Rep. 5 (2015) 1–12. doi:10.1038/srep11583.
- [22] H. Strathmann, Ion-exchange Membrana Separation Processes. Membrane Science and Technology Series 9, 1st ed., Elsevier Ltd, Amsterdam, 2004.
- [23] E.P. Rivero, A. Ortega, M.R. Cruz-Díaz, I. González, Modelling the transport of ions and electrochemical regeneration of the resin in a hybrid ion exchange/electrodialysis process for As(V) removal, J. Appl. Electrochem. 48 (2018) 597–610. doi:10.1007/s10800-018-1191-5.
- [24] R. Pärnamäe, S. Mareev, V. Nikonenko, S. Melnikov, N. Sheldeshov, V. Zabolotskii, et al., Bipolar membranes: A review on principles, latest developments, and applications, J. Memb. Sci. 617 (2021). doi:10.1016/j.memsci.2020.118538.
- [25] I.C. Bassignana, H. Reiss, Ion transport and water dissociation in bipolar ion exchange membranes, J. Memb. Sci. 15 (1983) 27–41. doi:10.1016/S0376-7388(00)81360-5.
- [26] V.I. Kovalchuk, E.K. Zholkovskij, E. V. Aksenenko, F. Gonzalez-Caballero, S.S. Dukhin, Ionic transport across bipolar membrane and adjacent Nernst layers, J. Memb. Sci. 284 (2006) 255–266. doi:10.1016/j.memsci.2006.07.038.

- [27] S. Mafé, P. Ramírez, A. Alcaraz, Electric field-assisted proton transfer and water dissociation at the junction of a fixed-charge bipolar membrane, Chem. Phys. Lett. 294 (1998) 406–412. doi:10.1016/S0009-2614(98)00877-X.
- [28] Q. Wang, B. Wu, C. Jiang, Y. Wang, T. Xu, Improving the water dissociation efficiency in a bipolar membrane with amino-functionalized MIL-101, J. Memb. Sci. 524 (2017) 370–376. doi:10.1016/j.memsci.2016.11.056.
- [29] J. Schiffbauer, N.Y. Ganchenko, G.S. Ganchenko, E.A. Demekhin, Overlimiting current due to electro-diffusive amplification of the second Wien effect at a cationanion bipolar membrane junction, Biomicrofluidics. 12 (2018). doi:10.1063/1.5066195.
- [30] C.O. Danielsson, A. Dahlkild, A. Velin, M. Behm, A model for the enhanced water dissociation on monopolar membranes, Electrochim. Acta. 54 (2009) 2983–2991. doi:10.1016/j.electacta.2008.12.025.
- [31] S.A. Mareev, E. Evdochenko, M. Wessling, O.A. Kozaderova, S.I. Niftaliev, N.D. Pismenskaya, et al., A comprehensive mathematical model of water splitting in bipolar membranes: Impact of the spatial distribution of fixed charges and catalyst at bipolar junction, J. Memb. Sci. 603 (2020) 118010. doi:10.1016/j.memsci.2020.118010.
- [32] A.I. Simion, C.G. Grigoraş, A.M. Roşu, L.V. Gavrilă, Mathematical modelling of density and viscosity of NaCl aqueous solutions, J. Agroaliment. Process. Technol. 21 (2015) 41–52.
- [33] J.P. Hershey, R. Damesceno, F.J. Millero, Densities and compressibilities of aqueous HCl and NaOH from 0 to 45 °C. The effect of pressure on the ionization of water, J. Solution Chem. 13 (1984) 825–848.
- [34] H. Ozbek, J.A. Fair, S.L. Phillips, Viscosity of aqueous sodium chloride solutions from 0 – 150 C, Lawrence Berkely Laboratory, University of California, Berkely, California, 1977.
- [35] E. Nishikata, T. Ishil, T. Ohta, Viscosities of hydrochloric acid solutions and viscosities of hydroiodic acid solutions, J. Chem. Eng. Data. 26 (1981) 254–256.

- [36] J. Olsson, A. Jernqvist, G. Aly, Thermophysical properties of aqueous NaOH-H₂O solutions at high concentrations, Int. J. Thermophys. 18 (1997) 779–793.
- [37] A. Bandura, S.N. Lvov, The ionization constant of water over wide ranges of temperatures and density, J. Phys. Chem. Ref. Data. 35 (2006) 15–30.
- [38] J. Newman, K.E. Thomas-Alyea, Electrochemical Systems, 3rd ed., Wiley-Interscience, New York, 2004.
- [39] B. Tjaden, S.J. Cooper, D.J. Brett, D. Kramer, P.R. Shearing, On the origin and application of the Bruggeman correlation for analysing transport phenomena in electrochemical systems, Curr. Opin. Chem. Eng. 12 (2016) 44–51. doi:10.1016/j.coche.2016.02.006.
- [40] Z. Zourmand, F. Faridirad, N. Kasiri, T. Mohammadi, Mass transfer modeling of desalination through an electrodialysis cell, Desalination. 359 (2015) 41–51. doi:10.1016/j.desal.2014.12.008.
- [41] M. Sharafan, V. Zabolotsky, Study of electric mass transfer peculiarities in electromembrane systems by the rotating membrane disk method, Desalination. 343 (2014) 194–197. doi:10.1016/j.desal.2013.12.023.
- [42] E. Al-Dhubhani, R. Pärnamäe, J.W. Post, M. Saakes, M. Tedesco, Performance of five commercial bipolar membranes under forward and reverse bias conditions for acid-base flow battery applications. J. Membrane Sci. (2021), in press. doi:10.1016/j.memsci.2021.119748.
- [43] T.A. Davis, J.D. Genders, D. Pletcher, A First Course in Ion Permeable Membranes, The Electrochemical Consultancy, Romsey, 1997.